Synthesis, Structural, Spectroscopic and Magnetic Studies of Two Azido and Thiocyanato Nickel(II) Dinuclear Complexes with Ferromagnetic Interactions†

Roberto Cortés,[a] J. I. Ruiz de Larramendi,[a] Luis Lezama,[a] Teófilo Rojo,*[,a] Karmele Urtiaga[b] and M. Isabel Arriortua[b]

[a] *Departamento de Química Inorgánica, Universidad del País Vasco, Aptdo. 644, 48080 Bilbao, Spain*

[b] *Departamento de Mineralogía-Petrología, Universidad del Pais Vasco, Aptdo. 644, 48080 Bilbao, Spain*

From a newly synthesised tridentate ligand [pepci = *N'*-(2-pyridin-2-ylethyl)pyridine-2-carbaldimine] two new octahedrally co-ordinated nickel(II) dimers, $[\{Ni(pepci)(N_3)_2\}_2]$ **1** and $[\{Ni(pepci)(NCS)_2\}_2]$ **2**, have been prepared. The crystal structure **1** has been solved. It crystallizes in space group $P2_1/c$ with four formula weights in a cell measuring a = 9.198(3), b = 17.382(6), c = 19.356(7) Å, and β = 99.57(1)°. The structure consists of isolated dimeric units in which the nickel ions are linked by two azide bridging groups in an end-on fashion. Two pepci ligands and two terminal azide groups complete the co-ordination spheres. Inside the dimer, each $Ni(pepci)(N_3)_2$ entity is crystallographically non-equivalent. There are two different bridging angles Ni(A)–N(4A)–Ni(B) 102.2(2) and Ni(B)–N(4B)–Ni(A) 101.0(2)°. The co-ordination geometry at each nickel atom is approximately octahedral. The Ni(A) ··· Ni(B) distance is 3.297(1) Å. For complex **2** a dimeric structure involving end-to-end thiocyanate bridging groups is proposed. Magnetic susceptibility data, measured from 4 to 300 K, were fitted to the Ginsberg equation, giving the parameters (cm^{-1}): J = +36.3, D = −18.8, $z'J'$ = 0.0 (N_3); and J = +4.9, D = −9.8, $z'J'$ = +0.33 (NCS). The magnetic behaviour of these and related complexes is discussed and some magnetostructural trends are given.

The synthesis and analysis of octahedrally co-ordinated di-bridged nickel(II) dimers have been the focus of several works.[1–4] The study of the intramolecular magnetic interactions in this type of compound helps to improve our understanding of the mechanisms of magnetic exchange on a structural basis using molecular orbital considerations.

The pseudohalide ions, specially azide and thiocyanate, show a great tendency to act as bridging ligands between two metallic centres.[5–8] Four bridging modes have been found for pseudohalide ligands in nickel(II) dimer compounds (**I** and **IV** are only observed for the azide ligand). If the superexchange interaction in mode **II** is propagated through a 90° pathway in the bridge, then exchange coupling *via* this mode of bridging could be ferromagnetic. In modes **I**, **III** and **IV** the superexchange does not go through an orthogonal bridge and the net interaction is generally antiferromagnetic. However, ferromagnetic interactions have also been found in compounds with this kind of bridging.

Magnetostructural correlations in these sorts of dimers are not easily identified because the superexchange mechanism is affected by a great number of structural parameters.[1–3] Ferromagnetic superexchange has been explained in terms of pathways which have an orthogonal interaction. A very interesting feature is the bridging angle required to attain this orthogonality, which is 90° for halide bridges but larger for other types of bridging atoms (oxygen, nitrogen etc.).

We have recently reported several nickel(II) dimers with 2,2′:6′,2″-terpyridine (terpy) and pseudohalide ligands.[9–11] It was shown that the bridging angles seem to play a significant role in determining the strength and sign of the exchange coupling constant in octahedrally co-ordinated nickel(II) dimers, with end-on or end-to-end pseudohalide bridging modes. Thus we have designed a synthetic strategy to obtain new polynuclear systems of Ni^{II}, with tridentate ligands (L_{III}), of general formula $[\{Ni(L_{III})X_2\}_2]\cdot nH_2O$ (X = pseudohalide).

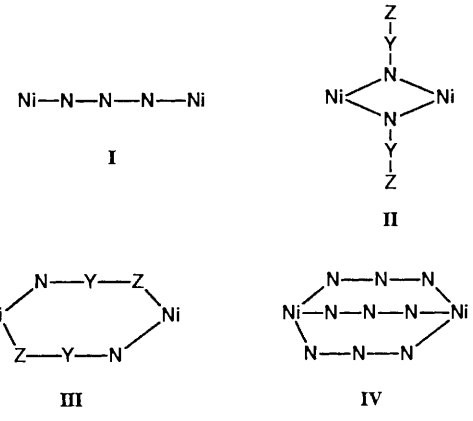

In order to determine the effect of varying the rigidity of the tridentate ligand on the disposition of the pseudohalide bridges and on the values of the bridging angles, we have decided to prepare several compounds with the *N'*-(2-pyridin-2-ylethyl)-pyridine-2-carbaldimine (pepci) [*N'*-(2-pyridin-2-ylethyl)-2-pyridylmethyleneamine] ligand. We here report the spectroscopic and magnetic properties of two new dibridged dimers formulated $[\{Ni(pepci)X_2\}_2]$ (X = N_3 or NCS) and the crystal structure of the azide complex. To delineate magnetostructural trends, both compounds are compared with several related nickel(II) dimers.

Experimental

Synthesis.—The pepci ligand was prepared by condensation

† *Supplementary data available:* see Instructions for Authors, *J. Chem. Soc., Dalton Trans.*, 1992, Issue 1, pp. xx–xxv.

of pyridine-2-carbaldehyde and 2-(2-aminoethyl)pyridine. To a solution of $[Ni(pepci)Cl_2]\cdot 2H_2O$ (previously prepared by reaction between $NiCl_2\cdot 6H_2O$ and pepci) in absolute methanol (0.100 g in 10 cm^3) were added aqueous saturated solutions (10 cm^3) of NaN_3 and KNCS respectively. The resulting green precipitates of $[Ni(pepci)(N_3)_2]$ **1** and $[Ni(pepci)(NCS)_2]$ **2** were filtered off, washed with water and dried over P_2O_5 for 48 h. Brown greenish prisms, suitable for X-ray analysis, were obtained by recrystallization from methanol–water solutions of compound **1**. All attempts to obtain good-quality crystals of compound **2** have not yet been successful (Found: C, 44.0; H, 3.6; N, 35.8; Ni, 16.5. $C_{13}H_{13}N_9Ni$ **1** requires C, 44.1; H, 3.7; N, 35.6; Ni, 16.6. Found: C, 46.5; H, 3.5; N, 18.2; Ni, 15.1. $C_{15}H_{13}N_5NiS_2$ **2** requires C, 46.7; H, 3.4; N, 18.1; Ni, 15.2%).

Physical Measurements.—Infrared spectra were monitored (in the 4000–250 cm^{-1} region) with a Perkin Elmer 1430 spectrophotometer, using KBr pellets, reflectance spectra on a Perkin Elmer lambda 9 spectrophotometer.

Magnetic susceptibility measurements were carried out, in the temperature range 4–300 K, using a DSM8 susceptometer/magnetometer equipped with a helium continuous-flow cryostat. For both compounds the independence of the magnetic susceptibility *versus* the applied field was checked at room temperature. The susceptibilities were corrected for diamagnetism [-148.5×10^{-6} (N_3) and -202.2×10^{-6} cm^3 mol^{-1} (NCS)] and for the temperature-independent paramagnetism estimated to be 100×10^{-6} cm^3 mol^{-1}.

Crystal Structure Determination.—Deep brown greenish blocks of $[Ni(pepci)(N_3)_2]$ **1**, grown from methanol–water, were sealed in glass capillaries before data collection. Preliminary cell dimensions were calculated by oscillation and Weisenberg photographs. Diffraction experiments were performed on an Enraf-Nonius CAD4 automatic diffractometer using graphite-monochromatized Mo-Kα radiation. The orientation matrix and the final lattice parameters were determined from 25 machine-centred high-angle reflections ($14 < 2\theta < 21°$). Machine parameters, crystal data, and data collection parameters are summarized in Table 1. The observed extinctions were consistent with the space group $P2_1/c$. Two standard reflections were recorded every 2 h. Their intensities showed no statistically significant change over the duration of data collection. Lorentz and polarization corrections were applied. The structure was solved using the direct methods, MULTAN 84[12] and successive Fourier syntheses (SHELX 76[13]). Non-hydrogen atomic scattering factors were taken from literature tables. In the refinement, all non-hydrogen atoms were assigned anisotropic thermal parameters while all hydrogen atoms were assigned isotropic thermal parameters. The hydrogen positions were located from Fourier difference map calculations. The final difference map revealed no peaks of chemical significance (maximum 0.59 and minimum -0.55 e $Å^{-3}$).

The geometric calculations were performed with XANADU[14] and molecular illustrations were drawn with SCHAKAL.[15]

Additional material available from the Cambridge Crystallographic Data Centre comprises H-atom coordinates, thermal parameters and remaining bond lengths and angles.

Results and Discussion

Synthetic Strategy for One-end and End-to-end Pseudohalide-bridged Nickel(II) Dimers.—The monomeric complexes of general formula $[Ni(L_{III})Cl_2]\cdot nH_2O$ (L_{III} = tridentate neutral ligand) can be considered as precursors in the synthesis of polynuclear nickel(II) systems with pseudohalide anions (X = N_3, NCS or NCO). The synthetic strategy is based on equilibria (1)–(3).

$$[Ni(L_{III})Cl_2]\cdot nH_2O(aq) + 2X^- \rightleftharpoons [Ni(L_{III})X_2]\cdot nH_2O(aq) + 2Cl^- \quad (1)$$

$$2[Ni(L_{III})X_2]\cdot nH_2O(aq) \rightleftharpoons [\{Ni(L_{III})X_2\}_2]\cdot nH_2O(s) \quad (2)$$

$$2[Ni(L_{III})X_2]\cdot nH_2O(aq) + 2PF_6^- \rightleftharpoons [\{Ni(L_{III})X_2\}_2][PF_6]_2\cdot nH_2O(s) + 2X^- \quad (3)$$

Both the tendency of nickel(II) ion to acquire six-coordination and the great capacity of the pseudohalide anions to act as bridging ligands would favour the stacking of $Ni(L_{III})X_2$ entities to give dimers. When azide ligand is used in these reactions the resulting dimer structure invariably shows end-on azide bridges, while if thiocyanate ligand is employed end-to-end bridges are obtained.[10,11] Both types of bridging in octahedrally co-ordinated nickel(II) dimers show ferromagnetic exchange coupling. The compounds formed with the cyanate ligand do not follow reaction (2) and stay as monomeric systems.[9] However, by following reaction (3), dimeric molecules formulated $[\{Ni(L_{III})(NCO)\}_2][PF_6]_2$ can be obtained by extraction of one pseudohalide (NCO) ligand.[9]

Crystal Structure.—Final positional parameters for the non-hydrogen atoms are listed in Table 2, bond distances and angles in Table 3. A SCHAKAL drawing of the dimeric $[\{Ni(pepci)(N_3)_2\}_2]$ complex is shown in Fig. 1.

The structure consists of isolated $[\{Ni(pepci)(N_3)_2\}_2]$ dimeric units, which are formed by the union of two $Ni(pepci)(N_3)_2$ crystallographically independent fragments. The two nickel(II) atoms are linked by two azide ions in an end-on bridging mode. The other two azide groups act as terminal ligands (Fig. 1). The co-ordination sphere at each nickel atom can be described as distorted octahedral, with the three nitrogen atoms of the pepci ligand [Ni–N 2.038(5)–2.114(6) Å] and the nitrogen atom from one bridging azide group [Ni(A)–N(4A) 2.107(5), Ni(B)–N(4B) 2.109(5) Å] in the equatorial plane, while the nitrogen atom of the terminal azide group [Ni(A)–N(7A) 2.077(7); Ni(B)–N(7B) 2.097(7) Å] and the nitrogen atom of the second azide bridging group [Ni(A)–N(4B) 2.163(6), Ni(B)–N(4A) 2.128(6) Å] occupy the axial positions. The four equatorial atoms of each nickel co-ordination sphere deviate significantly from planarity [-0.1371, $+0.1854$ Å for N(3A) and N(2A) respectively in plane A and -0.1906, $+0.1017$ Å for N(2B) and N(1B) respectively in plane B]. The nickel(II) ions are practically in the mean planes [deviations -0.0558 and 0.0535 Å for Ni(A) and Ni(B) respectively]. Distortions of the co-ordination polyhedra around the Ni^{II} from octahedral to the trigonal prismatic have been calculated by the Muetterties and Guggenberger model.[16] The resulting values of $\Delta = 0.036$ and 0.037 indicate that the polyhedra are close to octahedral.

Each of the pepci ligands is not planar due to the existence of two contiguous CH_2 groups forming angles close to 114°. This makes the two pyridine rings form dihedral angles of 27.9(2) and 23.1(2)° for the A and B units respectively. The bond lengths in the C(5),C(6),C(7) fragments show a good accord with the average bond length for a carbon–carbon single bond (1.505 Å); in the same way, the N(2)–C(8) bond length compares with that found for a double bond formed from similarly hybridized carbon and nitrogen atoms (1.273 Å). The disposition of the co-ordinated nitrogen atoms is practically planar. The shorter distances correspond to the two central N(2) atoms [2.038(5) (A unit) and 2.053(6) Å (B unit)].

The absence of an inversion centre that could correlate both halves of the dimer allows the existence of two different bridging angles [Ni(A)–N(4A)–Ni(B) 102.2(2) and Ni(B)–N(4B)–Ni(A) 101.0(2)°]. The two azide ligands of the bridging unit are not coplanar. They are quasi-linear [N(4A)–N(5A)–N(6A) 178.2(8) and N(4B)–N(5B)–N(6B) 179.5(8)°]. The nickel(II) ions are separated from each other by 3.297(1) Å. In the terminal N_3 groups the distances N(7A)–N(8A) and N(7B)–N(8B) are

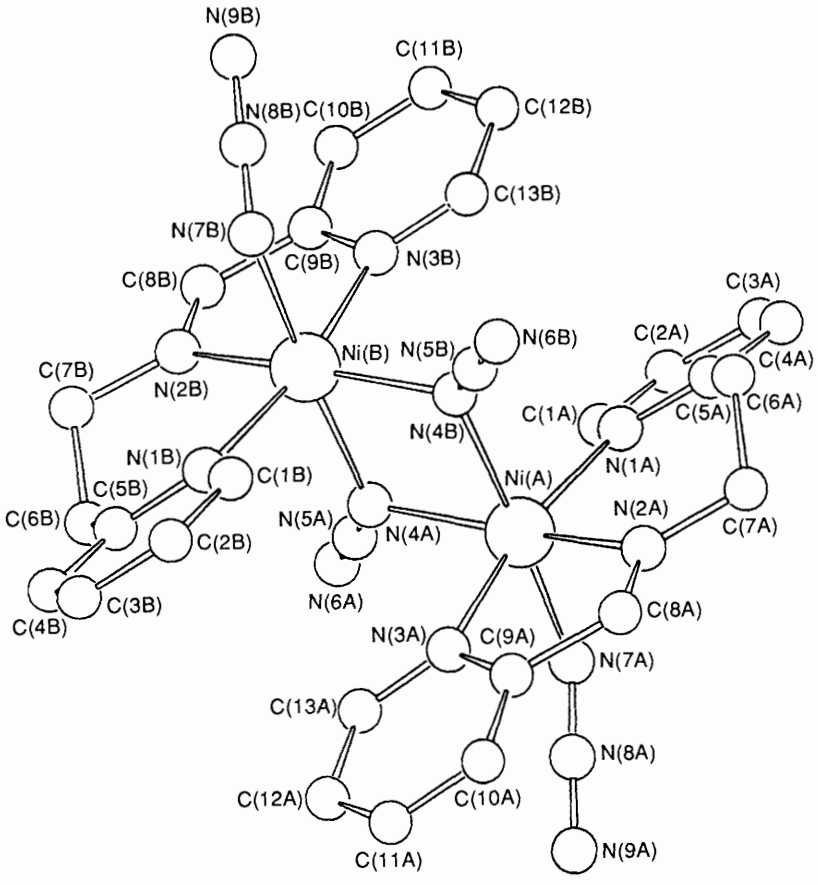

Fig. 1 Molecular structure of the dimeric compound $[\{Ni(pepci)(N_3)_2\}_2]$

Table 1 Data collection and structure refinement of $[\{Ni(pepci)(N_3)_2\}_2]$

Formula	$C_{26}H_{26}N_{18}Ni_2$
Dimensions/mm	0.45 × 0.32 × 0.27
M	707.42
System	Monoclinic
Space group	$P2_1/c$
a/Å	9.198(3)
b/Å	17.382(6)
c/Å	19.356(7)
β/°	99.57(1)
U/Å^3	3051(2)
Z	4
D_m/g cm^{-3}	1.56(2)
D_c/g cm^{-3}	1.54
μ(Mo-Kα)/cm^{-1}	12.9
F(000)	1456
λ(Mo-Kα)/Å	0.7107
Scan type	ω–2θ
θ Range/°	1.5–65
Check reflections	4 −1 −6, −2 −5 −6
No. measured reflections	6090
Interval h, k, l	10, 20, ±23
No. variables	494
Selection criterion	$I \geqslant 3\sigma(I)$
No. unique reflections	3454
p in $w = 1/[\sigma^2\|F_o\| + p\|F_o\|^2]$	0.001 54
$R = (\Sigma\|\|F_o\| - \|F_c\|\|)/(\Sigma\|F_o\|)$	0.067
$R' = [\Sigma w(\|F_o\| - \|F_c\|)^2/\Sigma w\|F_o\|^2]^{\frac{1}{2}}$	0.076

1.19(1) and 1.17(1) Å, while N(8A)–N(9A) and N(8B)–N(9B) are 1.14(1) and 1.16(1) Å, respectively. These ligands are quasi-linear with a N(7A)–N(8A)–N(9A) angle of 178(1)° and N(7B)–N(8B)–N(9B) 178.6(9)°. The greater difference observed between the N(7)–N(8) and N(8)–N(9) bond distances, in those terminal azides, for the A unit (1.19, 1.14 Å), compared with the B unit (1.17, 1.16 Å) can be explained by a larger π-donor effect in the A unit azide. It is in good accord with its greater Ni–N(7)–N(8) angle [123.4(5) (A), 120.6(5)° (B)].

Infrared Spectroscopy.—The position of the bands corresponding to the $\nu_{asym}(N_3)$ and ν(CN) stretching vibrations of the azide and thiocyanate pseudohalide groups can illustrate the mode of co-ordination to metal ions, because its energy depends on the degree of symmetry of these groups. The infrared spectrum of $[\{Ni(pepci)(N_3)_2\}_2]$ exhibits two bands, corresponding to $\nu_{asym}(N_3)$, at 2050 and 2020 cm^{-1}. The frequencies of these bands are similar to those exhibited by the related $[\{Ni(terpy)(N_3)_2\}_2]\cdot 2H_2O$ dimer,[10] which contains two terminal azide groups and two one-end azide bridging groups, showing a good accord with the structural results. The azide symmetric stretch, $\nu_{sym}(N_3)$, is observed at about 1300 cm^{-1} and the two signals at 620 and 605 cm^{-1} correspond to the azide bending vibrations (δ). In the case of $[\{Ni(pepci)(NCS)_2\}_2]$ the high frequencies observed for the bands corresponding to ν(CN), 2130 and 2100 cm^{-1}, are similar to those for the related $[\{Ni(terpy)(NCS)_2\}_2]$ which exhibits normal end-to-end NCS bridges,[17] being quite different to those observed for [Cu(paphy)(NCS)(SCN)] (paphy = pyridine-2-carbaldehyde 2′-pyridylhydrazone) which exhibits two unusual one-end thiocyanate-*N* bridging groups.[18] The band corresponding to the ν(CS) stretching vibration appears at 785 cm^{-1} and the δ(NCS) bending mode at 465 cm^{-1}.

UV/VIS *Spectra*.—The reflectance spectra of both complexes exhibit three defined bands at 10 750, 16 000, 26 000 and 10 800, 16 850, 26 000 cm^{-1} for the N_3 and NCS compounds respectively. These values are in agreement with those given in

Table 2 Fractional atomic coordinates ($\times 10^4$, $\times 10^5$ for Ni) for [{Ni(pepci)$(N_3)_2$}$_2$]

Atom	*X/a*	*Y/b*	*Z/c*	Atom	*X/a*	*Y/b*	*Z/c*
Ni(A)	43 545(9)	32 697(4)	90 936(4)	Ni(B)	57 797(9)	16 844(4)	85 513(4)
N(1A)	6 073(6)	3 476(3)	9 932(3)	N(1B)	4 054(7)	1 493(4)	7 709(3)
N(2A)	4 461(7)	4 367(3)	8 734(3)	N(2B)	5 649(8)	574(3)	8 898(4)
N(3A)	2 552(6)	3 268(3)	8 273(3)	N(3B)	7 555(7)	1 653(3)	9 399(3)
N(4A)	4 275(6)	2 065(3)	9 204(3)	N(4B)	5 870(6)	2 887(3)	8 422(3)
N(5A)	3 878(7)	1 754(3)	9 698(4)	N(5B)	6 224(7)	3 234(3)	7 946(4)
N(6A)	3 532(10)	1 446(4)	10 176(5)	N(6B)	6 565(10)	3 580(4)	7 476(4)
N(7A)	2 942(8)	3 507(4)	9 799(3)	N(7B)	7 260(8)	1 412(4)	7 873(3)
N(8A)	1 710(8)	3 724(4)	9 627(4)	N(8B)	8 407(8)	1 131(4)	8 089(4)
N(9A)	520(9)	3 936(5)	9 482(5)	N(9B)	9 529(9)	839(6)	8 297(6)
C(1A)	6 116(9)	3 051(5)	10 527(4)	C(1B)	3 958(9)	1 942(5)	7 136(4)
C(2A)	7 079(9)	3 189(5)	11 132(5)	C(2B)	2 920(9)	1 870(6)	6 532(4)
C(3A)	8 034(9)	3 801(6)	11 150(5)	C(3B)	1 913(9)	1 285(6)	6 521(5)
C(4A)	8 001(9)	4 244(5)	10 552(5)	C(4B)	2 013(9)	800(6)	7 096(5)
C(5A)	7 022(8)	4 067(4)	9 941(4)	C(5B)	3 038(9)	917(4)	7 680(4)
C(6A)	7 034(10)	4 535(5)	9 297(5)	C(6B)	3 090(12)	401(5)	8 338(6)
C(7A)	5 565(10)	4 924(5)	9 011(5)	C(7B)	4 588(10)	27(5)	8 593(6)
C(8A)	3 503(10)	4 521(5)	8 165(5)	C(8B)	6 613(10)	405(5)	9 458(6)
C(9A)	2 365(9)	3 946(4)	7 919(4)	C(9B)	7 710(8)	971(4)	9 735(4)
C(10A)	1 133(10)	4 079(6)	7 410(5)	C(10B)	8 910(10)	828(6)	10 261(5)
C(11A)	54(11)	3 524(7)	7 286(5)	C(11B)	9 985(10)	1 355(6)	10 420(5)
C(12A)	202(9)	2 855(6)	7 647(5)	C(12B)	9 833(10)	2 061(6)	10 066(5)
C(13A)	1 499(9)	2 738(5)	8 149(4)	C(13B)	8 595(8)	2 191(4)	9 555(4)

Table 3 Selected bond distances (Å) and angles (°) for [{Ni(pepci)$(N_3)_2$}$_2$]

Nickel co-ordination spheres			
Ni(A)–N(1A)	2.099(5)	Ni(B)–N(1B)	2.104(6)
Ni(A)–N(2A)	2.038(5)	Ni(B)–N(2B)	2.053(6)
Ni(A)–N(3A)	2.097(5)	Ni(B)–N(3B)	2.114(6)
Ni(A)–N(4A)	2.107(5)	Ni(B)–N(4B)	2.109(5)
Ni(A)–N(7A)	2.077(7)	Ni(B)–N(7B)	2.097(7)
Ni(A)–N(4B)	2.163(6)	Ni(B)–N(4A)	2.128(6)
Ni(A) · · · Ni(B)	3.297(1)	Ni(A) · · · Ni(B^I)	7.826(1)
Ni(B) · · · Ni(A^{II})	7.826(1)		
N(7A)–Ni(A)–N(1A)	86.0(2)	N(7B)–Ni(B)–N(1B)	87.9(2)
N(7A)–Ni(A)–N(2A)	96.3(3)	N(7B)–Ni(B)–N(2B)	94.1(3)
N(7A)–Ni(A)–N(3A)	89.8(2)	N(7B)–Ni(B)–N(3B)	89.0(2)
N(7A)–Ni(A)–N(4A)	95.4(2)	N(7B)–Ni(B)–N(4B)	96.1(2)
N(1A)–Ni(A)–N(2A)	91.8(2)	N(1B)–Ni(B)–N(2B)	91.5(3)
N(1A)–Ni(A)–N(3A)	170.0(2)	N(1B)–Ni(B)–N(3B)	169.4(2)
N(1A)–Ni(A)–N(4A)	97.2(2)	N(1B)–Ni(B)–N(4B)	96.0(2)
N(2A)–Ni(A)–N(3A)	79.6(2)	N(2B)–Ni(B)–N(3B)	78.6(2)
N(2A)–Ni(A)–N(4A)	165.7(2)	N(2B)–Ni(B)–N(4B)	167.5(3)
N(3A)–Ni(A)–N(4A)	92.2(2)	N(3B)–Ni(B)–N(4B)	94.4(2)
N(2A)–Ni(A)–N(4B)	90.6(2)	N(2B)–Ni(B)–N(4A)	91.1(3)
N(7A)–Ni(A)–N(4B)	173.0(2)	N(7B)–Ni(B)–N(4A)	174.8(2)
Ni(A)–N(4A)–Ni(B)	102.2(2)	Ni(B)–N(4B)–Ni(A)	101.0(2)
Bridging azides			
N(4A)–N(5A)	1.21(1)	N(4B)–N(5B)	1.191(9)
N(5A)–N(6A)	1.16(1)	N(5B)–N(6B)	1.18(1)
Ni(A)–N(4A)–N(5A)	123.1(5)	Ni(B)–N(4B)–N(5B)	128.0(5)
N(4A)–N(5A)–N(6A)	178.2(8)	N(4B)–N(5B)–N(6B)	179.5(8)

Symmetry relations: I $1-x, \frac{1}{2}+y, \frac{3}{2}-z$; II $1-x, -\frac{1}{2}+y, \frac{3}{2}-z$.

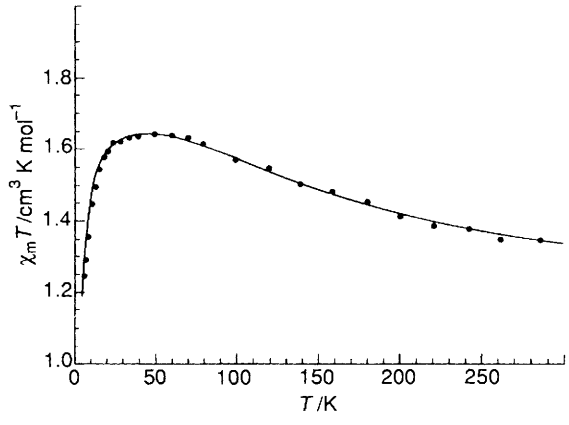

Fig. 2 Magnetic behaviour of [{Ni(pepci)$(N_3)_2$}$_2$]. The full line represents the curve calculated using the Ginsberg expression for a nickel(II) dimer

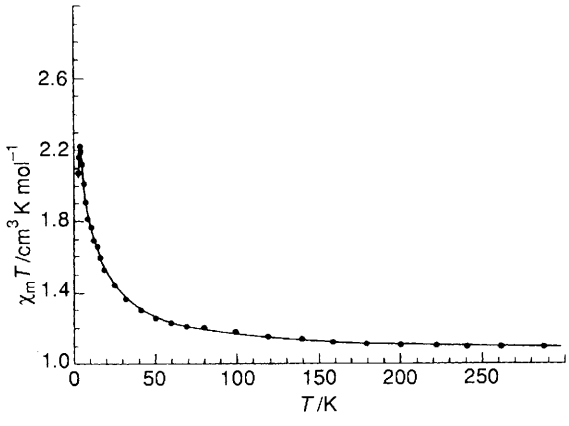

Fig. 3 Magnetic behaviour of [{Ni(pepci)$(NCS)_2$}$_2$]. Full line as in Fig. 2

the literature for octahedral nickel(II) compounds.[19,20] The bands have been ascribed to d → d transitions in a symmetry near to O_h [$^3A_{2g} \rightarrow {}^3T_{2g}, \rightarrow {}^3T_{1g}(F), \rightarrow {}^3T_{1g}(P)$], as indicated by the Δ distortion values. The nephelauxetic parameter β calculated[20] for the azide compound is 0.81, while for thiocyanate compound it is 0.85.

Magnetic Measurements.—The magnetic susceptibility of complexes **1** and **2** was measured throughout the temperature range 4.2–298 K. The results are illustrated in Figs. 2 and 3 as the thermal variation of the product $\chi_m T$.

The variation of the reciprocal molar magnetic susceptibility data *versus* temperature for **2** is well described, for temperatures higher than 50 K, by a Curie–Weiss law: $\theta = +14.5$ K

Table 4 Structural and magnetic parameters of octahedrally co-ordinated di-bridged nickel(II) dimers

End-on bridged compounds	Ni–X–Ni′/°	Ni · · · Ni′/Å	Ni–X/Å	X–Ni′/Å	J/cm^{-1}	D/cm^{-1}	d^a/Å	Ref.
$[Ni(terpy)(NCO)(H_2O)]_2[PF_6]_2$	97.7(3)	3.19(2)	2.04(2)	2.19(3)	+4.6	−12.2	0.01	9
$[\{Ni(terpy)(N_3)_2\}_2]\cdot 2H_2O$	101.3(3)	3.268	2.038(6)	2.198(8)	+20.1	−12.5	0.01	10
$[\{Ni(pepci)(N_3)_2\}_2]$	102.2(2)	3.297(1)	2.107(5)	2.128(6)	+36.3	−18.8	0.01	This
	101.0(2)		2.163(6)	2.109(5)				work
$[Ni_2(en)_4Cl_2]Cl_2$	96.6(4)	3.127	2.461(3)	2.551(3)	+6.6	−12.2	0.01	23, 24
$[\{Ni_2(en)_4Cl\}_2][ClO_4]_2$	95.4(3)	3.235	2.461(3)	2.512(3)	+8.9	−4.2	0.02	23, 24
$[H_2pd]_2[Ni_2(H_2O)_2Cl_8]$	95.0(5)	3.606	2.430(1)	2.459(1)	+8.1	−3.4	0.01	1
$[Ni_2(eg)_4Cl_2]Cl_2$	93.0(1)	3.458	2.383(1)	2.383(1)	+9.0	—	0.01	25

End-to-end bridged compounds	Ni–Z–Y/°	Y–N–Ni′/°	Ni · · · Ni′/Å	Ni–N/Å	Z–Ni′/Å	J/cm^{-1}	D/cm^{-1}	d^a/Å	Ref.
$[\{Ni(en)_2(NCS)\}_2]I_2$	100	167	5.78	2.04	2.61	+4.5	−3.3	0.05	26
$[\{Ni(tren)(NCS)\}_2][BPh_4]_2$	100	167	5.78	2.04	2.61	+2.4	−0.4	0.05	3
$[\{Ni(terpy)(NCS)_2\}_2]$	100.0(8)	159(2)	5.633(3)	2.04(2)	2.625(5)	+4.9	−4.3	0.56	11
$[\{Ni(pepci)(NCS)_2\}_2]$						+4.9	−9.8		This work
$[\{Ni(tren)(NCO)\}_2][BPh_4]_2$	117.1(5)	155.0(5)	5.385(1)	2.018(7)	2.336(5)	−4.4	−10.1	0.25	3, 21
$[\{Ni(tren)(N_3)\}_2][BPh_4]_2$	135.3(7)	122.3(3)	5.220(2)	2.069(8)	2.195(7)	−35.1	+6.8	0.52	22
$[\{NiL(N_3)_2\}_2]$	138.4(3)	124.4(2)		2.135(3)	2.167(3)	−90	0[b]	0.02	8

All the compounds except $[\{Ni(pepci)(N_3)_2\}_2]$ are centrosymmetric. X = N_3, NCO or Cl; NYZ = NCO, NCS or NNN. en = Ethane-1,2-diamine, pd = propane-1,3-diamine, eg = ethylene glycol and L = 1,5,9-triazacyclododecane.
[a] Deviation of Ni from plane of bridging ligand. [b] Magnetic susceptibility data have been analysed using the simple isotropic Heisenberg dimer model assuming a zero-field parameter $D = 0$.

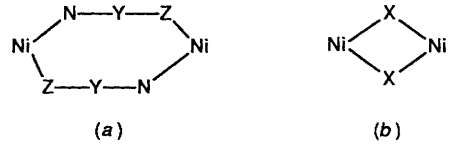

(*a*) (*b*)

Fig. 4 Schematic bridging units for end-to-end (*a*) and end-on (*b*) bridging modes (NYZ = N_3, NCO or NCS; X = N_3, NCO or Cl)

and $C = 1.02$ cm^3 K mol^{-1}. The $\chi_m T$ products for both compounds increase with decreasing temperature. For compound **1** saturation is reached at a value of 1.64 cm^3 K mol^{-1}, after which $\chi_m T$ decreases. In the case of compound **2** a maximum of 2.24 cm^3 K mol^{-1} is reached at 5.2 K and at lower temperatures $\chi_m T$ rapidly decreases. The magnetic susceptibility data have been analysed in terms of the theoretical equations for a nickel(II) dimer as put forth by Ginsberg *et al.*[2] This fit allows one to evaluate the intradimer exchange integral J, the nickel(II) single-ion zero-field splitting D, and the interdimer magnetic exchange J' for both compounds. The g values were fixed at 2.11 (N_3) and 2.06 (NCS), as determined from the Curie–Weiss plots. The calculated solid curves in Figs. 2 and 3 show excellent agreement with the observed values (points), yielding the following parameters (cm^{-1}): $J = +36.3$, $D = -18.8$, $z'J' = 0.0$ (N_3); $J = +4.9$, $D = -9.8$, $z'J' = +0.33$ (NCS).

As usual in this type of fitting the D and $z'J'$ parameters are approximations, because their effects are most important in the low-temperature region where the experimental uncertainties are greatest. However, the value of the exchange parameter J for a nickel(II) dimer is not influenced markedly by the value of either the zero-field splitting or the interdimer interaction, and appear accurately determined. This behaviour indicates the existence of an intradimer ferromagnetic exchange. The population of the molecular ground state $S = 2$ increases the value of $\chi_m T$ with decreasing temperature. The single-ion zero-field splitting results in a depopulation to a diamagnetic ground state and consequently the decrease in $\chi_m T$ at lower temperatures.

Table 4 compiles the structural and magnetic parameters of several octahedrally co-ordinated end-on or end-to-end pseudohalide-bridged nickel(II) dimers (in the case of end-on bridging compared with the corresponding halides). This has been made in order to study the relationship between the strength and sign of the exchange constant J and the structural parameters in these kinds of complexes.

End-to-end bridging mode. It has recently been established[11] that in octahedrally co-ordinated end-to-end bridged nickel(II) dimers the significant role in determining the net magnetic interaction is played by the bridging angles. The difference between the antiferromagnetic behaviour of the cyanate and azide tren [tris(2-aminoethyl)amine] dimers[21,22] and the ferromagnetic behaviour of the thiocyanate tren dimer[3] (see Table 4) was initially ascribed by Landee and Willett[1] to the separation of the nickel(II) ions with respect to the planes formed by the bridging groups. This separation is 0.05 Å for the thiocyanate–tren complex and ±0.25 and ±0.52 Å for the cyanate and azide tren dimers respectively. These larger separations in the latter compounds enhance the antiferromagnetic contributions by movement of the metal ions out of the bridging planes.[27] However, in the azide-bridged dimer $[\{NiL(N_3)_2\}]$ the eight-membered $Ni_2(\mu\text{-}N_3)_2$ ring is approximately planar and the compound exhibits the strongest antiferromagnetic behaviour ($J = -90$ cm^{-1}).[8] On the other hand, in the thiocyanate terpy complex the nickel ions lie ±0.56 Å out of the bridging plane, similar to the azide tren compound, and a ferromagnetic behaviour is observed.[11] These facts reveal that the separation of the metal ions from the bridging planes is not a determining factor in the net magnetic interactions. Table 4 shows that antiferromagnetic character grows as the Ni–Z–Y angle increases [Fig. 4(*a*)], away from orthogonality, and simultaneously the Y–N–Ni′ angle decreases towards 120° (optimum angle for nickel–pseudohalide overlap).[28] It can be also observed that each type of pseudohalide ligand shows characteristic bridging angles that favour a certain magnetic interaction. The strongest antiferromagnetic interactions correspond to the azide bridges whose symmetry imposes more similar angles deviating greatly from orthogonality. We note that the molecular structures of all the compounds lie on an inversion centre, except that corresponding to the pepci ligand.

End-on bridging mode. In the case of end-on pseudohalide-bridged nickel(II) compounds, the bridging network NiN_2Ni [Fig. 4(*b*)] allows the situation of accidental orthogonality to occur[28,29] to give ferromagnetic interactions. This situation takes place for very peculiar values of the structural parameters, which cannot be known exactly *a priori*. From Table 4 it can be seen that the Ni · · · Ni distance, which is so great, does not play a significant role in determining the net magnetic interaction. In all these compounds the nickel(II) ion is practically in the bridging plane. In the same way, we can say that the distortion around the nickel ion is not the cause of the different

strengths of the exchange integral, because the $[\{Ni(terpy)(NCO)(H_2O)\}_2][PF_6]_2$ and $[\{Ni(terpy)(N_3)_2\}_2]\cdot 2H_2O$ compounds,[9,10] having practically the same value for the zero-field splitting, show a great difference in the J value. The main factor may be ascribed then to the differences between the Ni–N–Ni bridging angles. If we consider these angles and the corresponding J values in the end-on bridged compounds shown in Table 4, it can be seen that for the related halide complexes the experimental bridging angle for orthogonality to occur is close to 90°; however, for the end-on pseudohalide bridges the orthogonality of the magnetic orbitals appears to be reached at values larger than 102.2°. This difference can be explained by the following considerations, taking into account the different contributions, with opposite signs, to the exchange integral, especially the antiferromagnetic ones.

In a bridging network as shown in Fig. 4(*b*) the main pathway for antiferromagnetic coupling takes place through the s orbitals of the bridging group, being less important for the 2s orbitals of the nitrogen atoms of the azide and cyanate groups than for the 3s chlorine orbitals. It results in the variation in the bridging angle for accidental orthogonality. When the X bridges are very electronegative (halide atom), the s valence orbitals of the bridges are too low in energy to interact with the metal orbitals, and the orthogonality bridging angle is very close to 90°. When X is made less electronegative (nitrogen atom of pseudohalide) the separation of the orbitals decreases and the interaction shifts the bridging angle to a larger value.

Conclusion

In both 'end-on' and 'end-to-end' modes the bridging angle plays a significant role in determining the net magnetic interactions for nickel(II) dimers. In the case of the end-on type the experimental bridging angle for orthogonality to occur is larger than 102.2°. Each type of pseudohalide ligand shows a rather characteristic value of the bridging angle for the end-to-end bridging mode. Logically the more symmetrical situation takes place for the azide group, and corresponds to the greater antiferromagnetic exchange coupling.

Acknowledgements

This work was financially supported in part by a grant (PB90-0549) from the Ministerio de Educación y Ciencia, Direccion General de Investigacion Cientifica y Tecnica which we gratefully acknowledge.

References

1 C. P. Landee and R. D. Willet, *Inorg. Chem.*, 1981, **20**, 2521.
2 A. P. Ginsberg, R. L. Martin, R. W. Brookes and R. C. Sherwood, *Inorg. Chem.*, 1972, **11**, 2884.
3 D. M. Duggan and D. N. Hendrickson, *Inorg. Chem.*, 1974, **13**, 2929.
4 T. Rojo, L. Lezama, R. Cortés, J. L. Mesa, M. I. Arriortua and G. Villeneuve, *J. Magn. Magn. Mater.*, 1990, **83**, 519.
5 E. J. Laskowsky, D. M. Duggan and D. N. Hendrickson, *Inorg. Chem.*, 1975, **14**, 2449.
6 G. R. Hall, D. M. Duggan and D. N. Hendrickson, *Inorg. Chem.*, 1975, **14**, 1956.
7 O. P. Anderson, A. B. Packard and M. Wicholas, *Inorg. Chem.*, 1976, **15**, 1613.
8 P. Chaudhuri, M. Guttmann, D. Ventur, K. Weighardt, B. Nuber and J. Weiss, *J. Chem. Soc., Chem. Commun.*, 1985, 1618.
9 M. I. Arriortua, R. Cortés, J. L. Mesa, L. Lezama, T. Rojo and G. Villeneuve, *Transition Met. Chem.*, 1988, **13**, 371.
10 M. I. Arriortua, R. Cortés, L. Lezama, T. Rojo, X. Soláns and M. Font-Bardía, *Inorg. Chim. Acta*, 1990, **174**, 263.
11 T. Rojo, R. Cortés, L. Lezama, M. I. Arriortua, K. Urtiaga and G. Villeneuve, *J. Chem. Soc., Dalton Trans.*, 1991, 1779.
12 P. Main, G. Germain and M. M. Woolfson, MULTAN 84, A system of Computer Programs for the Automatic Solution of Crystal Structures from X-ray Diffraction Data, Universities of York and Louvain, 1984.
13 G. M. Sheldrick, SHELX 76, Program for Crystal Structure Determination, University of Cambridge, 1976.
14 P. Roberts and G. M. Sheldrick, XANADU, Program for Torsion Angle, Mean Plane and Libration Correction Calculations, University of Cambridge, 1975.
15 E. Keller, SCHAKAL 88, A Fortran Program for the Graphic Representation of Molecular and Crystallographic Models, University of Freiburg, 1988.
16 E. L. Muetterties and L. J. Guggenberger, *J. Am. Chem. Soc.*, 1974, **96**, 1748.
17 T. Rojo, R. Cortés, L. Lezama, J. L. Mesa and G. Villeneuve, *Inorg. Chim. Acta*, 1989, **162**, 11.
18 J. L. Mesa, T. Rojo, M. I. Arriortua, G. Villeneuve, J. V. Folgado, A. Beltrán and D. Beltrán, *J. Chem. Soc., Dalton Trans.*, 1989, 53.
19 W. Henke and D. Reinen, *Z. Anorg. Allg. Chem.*, 1977, **436**, 187.
20 A. B. P. Lever, *Inorganic Electronic Spectroscopy*, Elsevier, Amsterdam, 1986.
21 D. M. Duggan and D. N. Hendrickson, *Inorg. Chem.*, 1974, **13**, 2056.
22 C. G. Pierpont, D. N. Hendrickson, D. M. Duggan, F. Wagner and E. K. Barefield, *Inorg. Chem.*, 1975, **14**, 604.
23 Y. Journeaux and O. Kahn, *J. Chem. Soc., Dalton Trans.*, 1979, 1575.
24 G. A. Bottomley, L. G. Glossop, C. L. Raston, A. H. White and A. C. Willis, *Aust. J. Chem.*, 1978, **31**, 285.
25 D. Knetsch and W. L. Groeneveld, *Inorg. Nucl. Chem. Lett.*, 1976, **12**, 27.
26 A. E. Shvelashvili, M. A. Porai-Koshits and A. S. Antsyshkina, *J. Struct. Chem. (Engl. Transl.)*, 1969, **10**, 552.
27 A. Bencini and D. Gatteschi, *Inorg. Chim. Acta*, 1978, **31**, 11.
28 O. Kahn and M. F. Charlot, *Nouv. J. Chim.*, 1980, **4**, 567.
29 V. M. Crawford, H. W. Richardson, J. R. Wasson, D. J. Hodgson and W. E. Hatfield, *Inorg. Chem.*, 1976, **15**, 2107.

Received 22*nd April* 1992; *Paper* 2/02061K